NANO LETTERS

pubs.acs.org/NanoLett

Letter

Flexible Ultrathin Single-Crystalline Perovskite Photodetector

Hao Jing, Ruwen Peng,* Ren-Min Ma,* Jie He, Yi Zhou, Zhenqian Yang, Cheng-Yao Li, Yu Liu, Xiaojiao Guo, Yingying Zhu, Di Wang, Jing Su, Cheng Sun, Wenzhong Bao, and Mu Wang*

Cite This: *Nano Lett.* 2020, 20, 7144−7151

Read Online

ACCESS | Metrics & More | Article Recommendations | Supporting Information

ABSTRACT: Flexible optoelectronic devices attract considerable attention due to their prominent role in creating novel wearable apparatus for bionics, robotics, health care, and so forth. Although bulk single-crystalline perovskite-based materials are well-recognized for the high photoelectric conversion efficiency than the polycrystalline ones, their stiff and brittle nature unfortunately prohibits their application for flexible devices. Here, we introduce ultrathin single-crystalline perovskite film as the active layer and demonstrate a high-performance flexible photodetector with prevailing bending reliability. With a much-reduced thickness of 20 nm, the photodetector made of this ultrathin film can achieve a significantly increased responsivity as 5600A/W, 2 orders of magnitude higher than that of recently reported flexible perovskite photodetectors. The demonstrated 0.2 MHz 3 dB bandwidth further paves the way for high-speed photodetection. Notably, all its optoelectronic characteristics resume after being bent over thousands of times. These results manifest the great potential of single-crystalline perovskite ultrathin films for developing wearable and flexible optoelectronic devices.

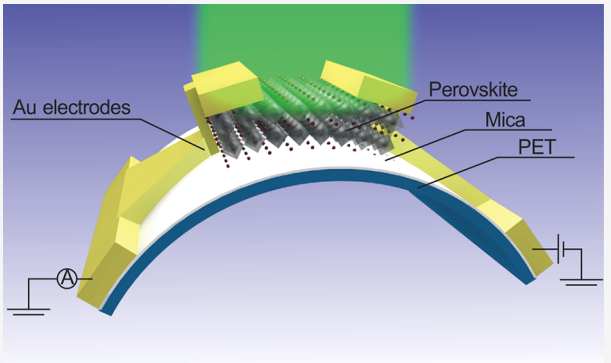

KEYWORDS: *Flexible photodetector, single-crystalline perovskite, ultrathin film, hybrid organic−inorganic perovskite*

INTRODUCTION

The flexible photodetector (PD) is a crucial active component for wearable devices, foldable displays, and biomedical imaging systems.[1−6] It requires photoactive materials with high photoelectric conversion efficiency and comparable compliance.[7−11] Among the existing materials, hybrid organic−inorganic perovskites (HOIPs, the molecular formula of $CH_3NH_3PbX_3$ (X = Cl, Br, I)) emerge as a promising candidate, largely due to their exceptionally high optical absorption coefficient, long electron−hole diffusion length, high carrier mobility, and tunable bandgap.[12−17] Furthermore, HOIPs can be fabricated via the solution process,[18−22] eliminating the need for high processing temperature that can potentially be harmful to the flexible substrates. To date, HOIP-based flexible photodetectors, flexible image sensors, and wearable equipment have been widely reported.[23−28] However, in previous reports the perovskite materials are usually polycrystalline. Comparing with single-crystalline perovskite materials, the polycrystalline ones have larger charge trap density, shorter carrier lifetime, and lower carrier mobility.[29−31] Moreover, grain boundaries in the polycrystalline perovskites further compromise their structural stability at elevated ion migration or environmental humidity level.[32,33] Single-crystalline perovskite can significantly enhance device performance.[34,35] However, the stiff and brittle nature of single-crystalline perovskite materials is not readily compatible with the intended application for flexible photodetector.

It has been discovered recently[36−38] that the mechanical properties of a material can be significantly improved when the dimension is scaled down to the nanometer. Here, we demonstrate an additional example that a high-performance flexible photodetector can be realized by using ultrathin single-crystalline perovskite film. We developed a quasi-static solution synthesis approach to fabricate single-crystalline perovskite $CH_3NH_3PbBr_3$ as an active layer 20 nm in thickness on atomically flat mica sheet. The flexible photodetector made of 20 nm thick single-crystalline perovskite possesses significantly enhanced responsivity reaching 5600 A/W, more than 2 orders of magnitude higher than recently reported flexible perovskite photodetectors.[39−42] With the demonstrated fast temporal response as 3.2 μs rise-time and 9.2 μs fall-time, our flexible photodetector features 3 dB bandwidth from DC to 0.2 MHz. The reliability of flexible photodetector upon repeated bending is further validated experimentally. No visible deterioration in photocurrent and on/off switching ratio has been observed after 1000 bending cycles. In contrast, using the same testing

Received: June 15, 2020
Revised: September 2, 2020
Published: September 17, 2020

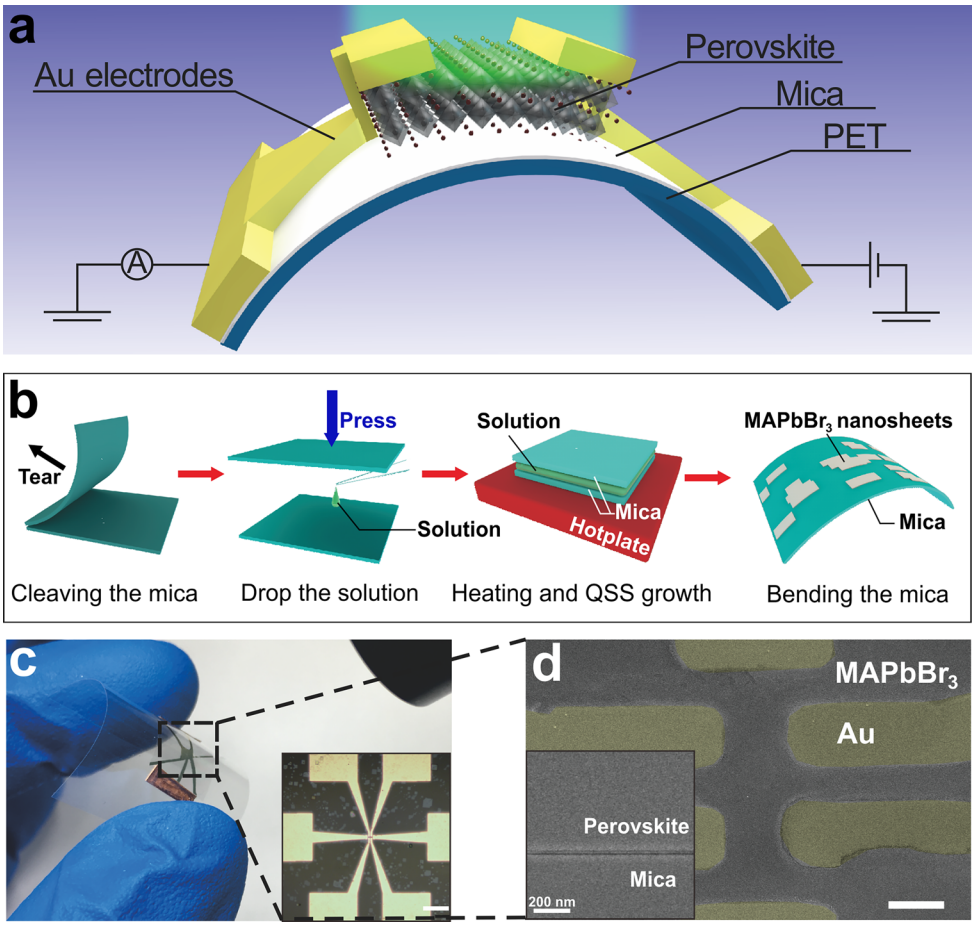

Figure 1. Architecture of the flexible photodetector and the characterization of the active layer. (a) Schematic of the device. (b) Schematic representations of the solution growth including the following four steps: (i) cleaving the mica; (ii) drop the solution between the micas; (iii) heating and quasi-static solution (QSS) growth; (iv) bending the mica substrate. (c) Photograph of the device. Inset: micrograph of the device, and the scale bar is 100 μm. (d) False-color SEM image of the device, where light yellow outlines the Au electrodes, and the scale bar is 3 μm. Inset: tilted SEM image of the edge of the perovskite nanosheet on mica.

protocol, the control samples with increased thickness of 202 and 809 nm show 21% and 49% reduction in photocurrent, respectively. Thus, the reported solution-based synthesis process enables low-cost fabrication of a high-performance flexible photodetector all at room temperature. It can be readily integrated into a wide range of flexible optoelectronic devices, such as artificial eyes, portable detectors, flexible smartphones, and so forth.

Fabrication and Photodetecting Characteristics. A flexible perovskite photodetector consists of an ultrathin single-crystalline perovskite $CH_3NH_3PbBr_3$ nanosheet atop of a flexible polyethylene terephthalate (PET) substrate with an interlayer of mica, as illustrated in Figure 1a. To grow the ultrathin single-crystalline perovskite $CH_3NH_3PbBr_3$ nanosheets, we employ two freshly cleaved mica sheets to make a confined growth space.[43−45] The growth space is slowly heated for a quasi-static synthesis process (Figure 1b)[43,46] (Supporting Information S1). The mica sheets act as flexible substrates in the growth of the ultrathin single-crystalline film. The mica sheet possesses an atomically smooth surface,[47] excellent wettability,[48] and low-chemical activity which promote the lateral growth and enlarge the crystal sheet.[49] The trap state density of the nanosheets is ~2.6×10^{11} cm^{-3} based on space-charge limited current analysis (Supporting Information S2), which is 5−6 orders of magnitude lower than the polycrystalline perovskite film.[50,51] Figure 1c,d shows optical and scanning electron micrographs of a fabricated device based on a single-crystalline perovskite with a smooth surface free of grain boundaries (more details in Supporting Information S2). The channel length of the photodetector is 2.6 μm.

Figure 2a shows the current−voltage (I−V) curves of a device under different illumination conditions. The photocurrent increases as the illumination intensity increases, and the maximum value reaches 0.34 μA at 1.12 mW/cm^2 with a biased voltage of 1.0 V. Figure 2b shows the corresponding responsivities as a function of illumination intensity. The responsivity is ~5600 A/W at 0.08 mW/cm^2, which is more than 2 orders of magnitude higher than reported flexible perovskite photodetectors (for example, see Table 1). It is also worthwhile to mention that this device possesses remarkable long-term stability, which can normally work more than 2 weeks after encapsulation by a poly(methyl methacrylate) coating, as shown in Supporting Information S3.

Specific detectivity (D^*) characterizes the ability of the photodetector to detect weak signals.[52] By measuring the noise current density spectra,[53] we can get $D^* = \frac{\sqrt{A\Delta f}}{NEP} = \frac{\sqrt{A\Delta f}}{i_n / R}$ where A is the effective area, Δf is the electric bandwidth, NEP is the noise equivalent power, and i_n is the noise current, and R is the responsivity. For the responsivity at the bias of 1 V and

https://dx.doi.org/10.1021/acs.nanolett.0c02468
Nano Lett. 2020, 20, 7144−7151

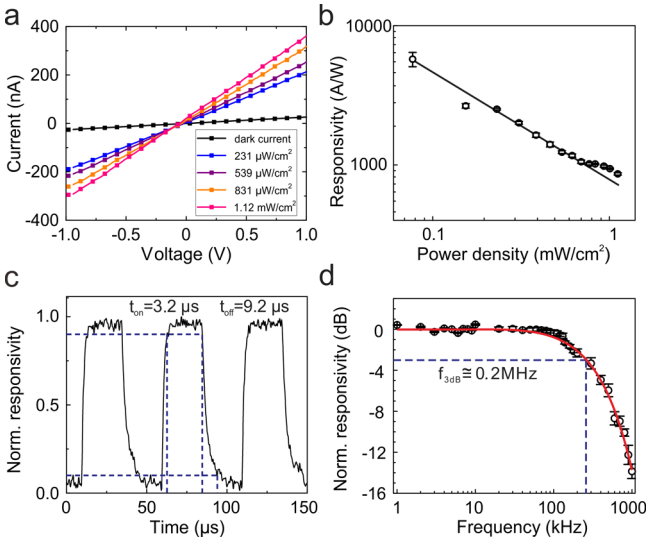

Figure 2. Photodetecting characterizations. (a) $I-V$ curves of the device at different power intensity of a 514 nm laser illumination. (b) The responsivity varies with the light intensity with a bias of 1 V. (c) The time domain response of the photocurrent with a bias of 2 V at the illumination with a 20 kHz modulation. (d) The normalized response as a function of input signal frequency at the bias of 2 V, showing the 3 dB bandwidth of the device is about 0.2 MHz.

the illumination intensity of 0.08 mW/cm^2, the corresponding specific detectivity is 6.59 × 10^{11} cm Hz$^{0.5}$ W^{-1} (Jones) as summarized in Table 1.

To extract the response time of our device, we measure the transient photocurrents where the device is illuminated by a frequency-doubled Ti:sapphire laser modulated by an acoustic optical modulator (see Methods). As shown in Figure 2c, the photocurrent rises and decays with a modulated laser pulse. The rise and fall time are 3.2 and 9.2 μs, respectively, at a 20 kHz modulation. More measured data at the modulation frequency ranging from 1 kHz to 1 MHz are given in Supporting Information S3. Further, Figure 2d illustrates the normalized responsivity versus the modulation frequency of the laser, which indicates a 3 dB bandwidth up to 0.2 MHz.

Mechanical Flexibility and Performance Comparison. We demonstrate the mechanical flexibility of the photodetector by bending the substrate to various radii as illustrated in the inset of Figure 3a. Figure 3a shows the $I-V$ curves of the

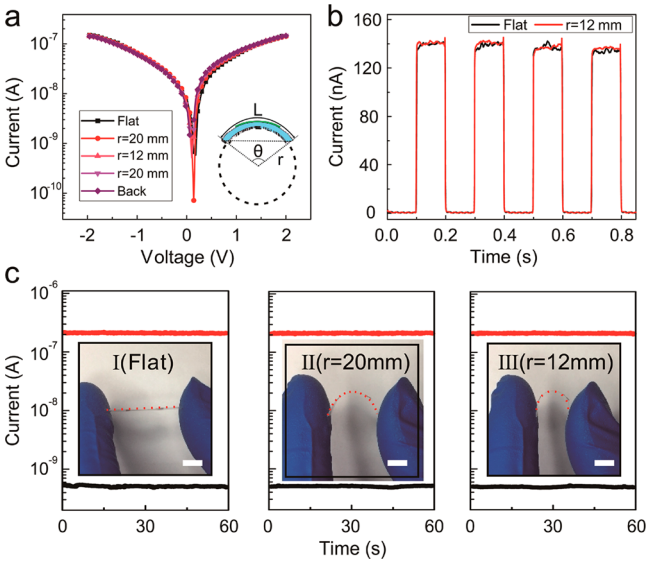

Figure 3. Mechanical flexibility and bending stability. (a) $I-V$ curves of the device as a function of bending radius. Inset: Schematic of the bending process. (b) $I-t$ curves of the photodetector exposed to pulsed light illumination (5 Hz) before and after the bending at the bias of 2 V. (c) Photocurrents and dark currents of the flexible photodetector at different bending radii at a bias of 2 V. Red line represents the photocurrent, while dark line represents the dark current. Inset: photographs of corresponding bending states; all of the scale bars represent 1 cm. All of the currents were measured under 514 nm laser illumination with the power density of 0.2 mW/cm^2 at ambient conditions.

Table 1. Comparison of the Performance of the Flexible PD Based on Ultrathin Single-Crystalline $MAPbBr_3$ Sheet with That of Other Flexible Perovskite PDs Reported in the Literatures

device structure	material structure	D^* [Jones]	responsivity [A/W]	rise/decay time [ms]	device area	on/off ratio	ref
Au/$MAPbBr_3$/Au	ultrathin single crystal ~20 nm	6.59 × 10^{11}	5600@1 V@514 nm	0.003/0.009	36 μm^2~100 μm^2	200	this work
$CsPbBr_3$/CNTS	nanosheets dispersions		31.1@10 V	0.016/0.38	26 μm^2	823	55
ITO/$MAPbI_3$/ITO	film		3.49@3 V@365 nm	<100/100	0.15 mm^2	152	23
Au/$MAPbI_3$/Au	microwires	5.25 × 10^{12}	13.57@-5 V@420 nm	0.08/0.24	3.78 × 10^3 μm^2		25
ITO/$MAPbI_3$/Au	nanowires	10^{10}	>0.03@0.3 V@500 nm	20.47/13.81	164 mm^2		26
TiO_2/Pero-Spiro/Au	spiro	3.61 × 10^{12}	21.5@0.6 V@350 nm	<200/200	7.1 mm^2	79.1	27
ITO/$CsPbBr_3$/ITO	nanosheets dispersions		0.64@10 V@517 nm	0.019/0.024	0.2 mm^2	>10^4	39
Au/$MAPbI_3$/Au	film	1.22 × 10^{13}	0.418@1 V		1.5 mm^2		40
ITO/$MAPbI_3$/ITO	film	>10^{11}	81@1 V@680 nm	0.23/0.38	0.9 mm^2	100	41
$MAPbI_3$/UCns/Au	film	0.76 × 10^{12}	0.27@2 V@980 nm	52/67	0.27 mm^2	>10^3	42
Au/$MAPbI_3$/Au	nanowire network	1.02 × 10^{12}	0.1@10 V@650 nm	0.3/0.4	0.1 mm^2	300	54
$MAPbI_3$/CNY	wire-shaped	1.76 × 10^{11}	10.2@0 V@617 nm	393/132		45	56
Au/$CsPbBr_3$/Au	microflake		2.776@5 V@275 nm	40/20			57
Au/$(PEA)_2PbI_4$/Au	membrane	1.62 × 10^{15}	98.17@4 V@460 nm	0.064/0.052	0.0454 mm^2		58
Al_2O_3/ $CsPbBr_3$/TiO_2	film	1.88 × 10^{13}	0.44@0 V@405 nm	0.028/0.27			59
Kapton/PbI_2:$Pb(SCN)_2$	nanowires	7.3 × 10^{12}	0.62@10 V	0.227/0.215	456 mm^2		60
$CsPbBr_3$/MXene	nanosheets	6.4 × 10^8	0.045@10 V@450 nm	48/18	80 mm^2	2.3 × 10^3	61
$MAPbI_3$/C8BTBT	network	2.17 × 10^{12}	8.1@3 V@532 nm	7.1/6.5		9.75 × 10^3	62

https://dx.doi.org/10.1021/acs.nanolett.0c02468
Nano Lett. 2020, 20, 7144−7151

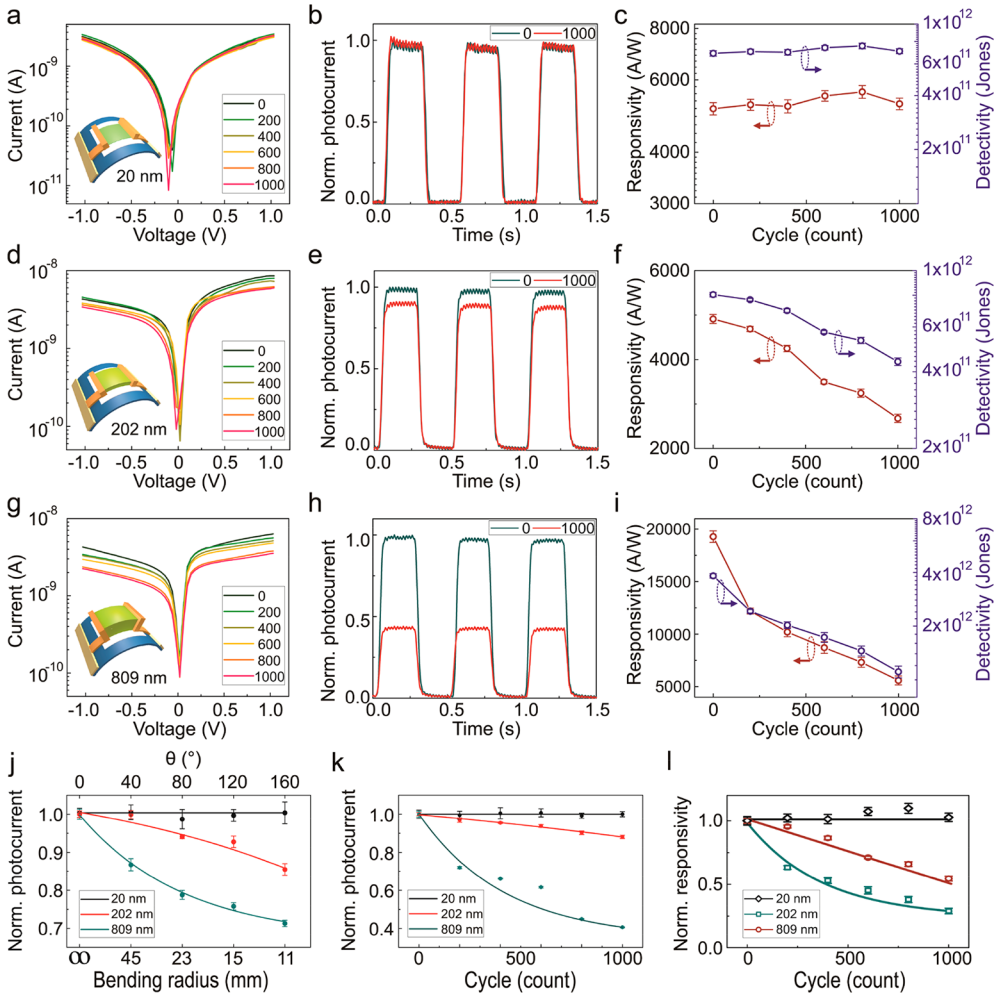

Figure 4. Photoelectrical responses of flexible PDs based on $MAPbBr_3$ sheets with different thickness. (a) $I-V$ curves, (b) $I-t$ curves, (c) the responsivity and detectivity of an ultrathin (20 nm in thickness) photodetector under 1000 times of bending cycles. (d) $I-V$ curves, (e) $I-t$ curves, (f) the responsivity and detectivity of a 202 nm thick photodetector under 1000 times of bending cycles. (g) $I-V$ curves, (h) $I-t$ curves, (i) the responsivity and detectivity of an 809 nm thick photodetector under 1000 times of bending cycles. (j) The normalized photocurrents of three samples with different thickness as a function of bending radius. (k) The normalized photocurrents of three samples with different thickness as a function of cyclic counts. (l) The normalized responsivities (the same as normalized detectivities) of three samples with different thickness as a function of cyclic counts. All of the $I-V$ and $I-t$ curves were measured under a broadband halogen lamp with the power density of 10.5 mW/cm^2 at ambient conditions, which are different from the cases in Figure 2a and Figure 3. $I-t$ curves were measured at the bias voltage of 2 V under the illumination with 2 Hz modulation. All of the responsivity and detectivity were measured under a 514 nm laser with the power density of 0.08 mW/cm^2 at ambient conditions.

device as a function of bending radius under 514 nm laser illumination (0.2 mW/cm^2) at ambient conditions. The flexible photodetector can be bent from a flat state to a radius of 12 mm and back to a flat state without any significant loss in responses of photocurrent. Figure 3b plots the photoresponses versus time characteristics ($I-t$) of the photodetector exposed to pulsed laser illumination before and after the bending, wherein the on/off switching ratio of ~200 is invariant of bending. These results indicate that the ultrathin single-crystalline perovskite photodetector yields great mechanical flexibility. Besides, to investigate the stability of the device after flexure the photodetector was held in bent states for 1 min at each measured radius under laser illumination at ambient conditions. As shown in Figure 3c, the photocurrents and dark currents both have no obvious changes at various radii, indicating that this photodetector possesses robust bending stability.

Comparing with recently reported flexible perovskite photodetectors working in the visible range (summarized in Table 1), our flexible photodetector exhibits several characteristics: (i) Ultrathin active layer with 20 nm in thickness, which is the thinnest flexible perovskite photodetector to the best of our knowledge. (ii) High responsivity up to 5600 A/W, much higher than that of previously reported flexible perovskite photodetectors for 2 orders of magnitude,[54−58] which demonstrates the remarkable detection efficiency of the photodetector. (iii) Fast response with the rise/fall time of 3.2/9.2 μs, which gives rise to an outstanding 3 dB bandwidth up to 0.2 MHz. The quick response of the device demonstrates the potential in high-speed detections and optical communications. (iv) Specific detectivity with the value of 6.59×10^{11} Jones is comparable with previous work,[59−62] which could be further enhanced by suppressing the dark current.

Thickness-Dependent Performance. The mechanical flexibility and bending stability of this single-crystalline

https://dx.doi.org/10.1021/acs.nanolett.0c02468
Nano Lett. 2020, 20, 7144−7151

perovskite photodetector are quite interesting since the single-crystalline perovskite material is often considered as a kind of fragile material, which is easily damaged by a variety of mechanical deformations including bending, compression, and tension.[63,64] Here, we compare the bending durability of the ultrathin photodetector (20 nm in thickness) with two control samples with much thicker active layers (202 and 809 nm in thickness), and more examples are provided in Supporting Information S4. All of these photodetectors are fixed on the mechanical bending machine and bent for 1000 times (from flat to the bending radius of 11 mm). Figure 4a,b plots the $I-V$ and $I-t$ curves of the ultrathin device (20 nm in thickness) as a function of bending cycles. No visible deterioration has been detected in photocurrent and on/off switching ratio after the bending test for 1000 times. Figure 4c plots the responsivity and detectivity of this ultrathin device as a function of bending cycles. Here the detectivity of the device is obtained based on the measured noise currents (Supporting Information S4). We can see that both the responsivity and the detectivity of the device remain quite stable during the bending process. This result indicates that the photodetector with ultrathin active layer yields outstanding bending durability.

For comparison, the photodetector with a 202 nm thick active layer possesses an obvious degeneration in the photocurrents at the bias of −1 V for ∼21% after 1000 time bending as shown in Figure 4d. Correspondingly, the on/off switching ratio decreases for ∼10% shown in $I-t$ curves as plotted in Figure 4e. In addition, the responsivity and detectivity of the device present an obvious decline in the bending process as illustrated in Figure 4f (∼45%). Furthermore, for the photodetector with an 809 nm thick active layer the photocurrents varied from 4.3 to 2.2 nA at the bias of −1 V for bending 1000 times (Figure 4g), which means an ∼49% degradation. The decrease in the photocurrents also leads to an obvious degeneration in the on/off switching ratio as shown in Figure 4h (∼56%) and in the responsivity (or the detectivity) as shown in Figure 4i (∼70%). These results demonstrate that the thinner the active layer, the less degradation in the photoresponse will be induced after the repeated bending cycles.

Figure 4j shows that the normalized photocurrents varies with a bending radius of three devices with different thicknesses. For the ultrathin device (thickness of 20 nm), there is no obvious degradation in the photocurrents during the bending. However, for the thick samples the photocurrents drop along with the decrease of bending radius, while the decrease for the 809 nm thick sample (∼29%) is much more intense than that for the 202 nm thick sample (∼15%). This result demonstrates that the mechanical flexibility of the single-crystalline perovskite photodetector gradually decreases following the increase of the thickness of the active layer. Furthermore, the degradation of the photocurrents gradually accumulates during the repeated bending process and results in significant performance degradation summarized in Figure 4k,l. However, the 3 dB bandwidths of the devices with different thicknesses (Supporting Information S4) have no obvious variation during the bending process for all devices with different thicknesses.

Our results demonstrate that the reduction in the thickness of the single-crystalline perovskite effectively promotes the flexibility and bending durability of the flexible photodetectors. This effect can be interpreted by the induced strain in bending; the strain on the top surface of the sheet was directly proportional to the thickness of the crystal, and the flexural rigidity was inversely proportional to the thickness of the sample.[65] Therefore, thicker sheets suffer stronger strain, which decreases their bending reliability. Optical measurements were also taken to prove the damage brought from strain. Although optical absorption of the sheets is less affected by the bending (Supporting Information S2), the decrease in the photoluminescence (PL) intensities and the variations in the PL peak positions are both more severe for thicker samples after thousands of times of bending (Supporting Information S5).

CONCLUSION

We report here a low-cost quasi-static solution-based approach to grow ultrathin single-crystalline perovskite materials. At the significantly reduced thickness of 20 nm, the brittle material has been transformed into a highly flexible sheet without compromising its excellent photoelectric conversion efficiency. We have demonstrated that a flexible photodetector using the ultrathin single-crystalline film as the active material achieves a record-high photoelectric responsivity of 5600 A/W, 2 orders of magnitude higher than that made of polycrystalline perovskite. The reduced thickness of the single-crystalline perovskite film also enhances its temporal response, resulting in a broadband photodetection from DC to 0.2 MHz. These data open up a promising potential in fabricating high-performance flexible optoelectronic devices for bionics, robotics, health care, and so forth.

METHODS

Synthesis of Perovskite. A 0.8 mol/L $MAPbBr_3$ solution was prepared by dissolving $MAPbBr_3$ powder in DMF. Six microliters of the solution was dropped onto a freshly cleaved mica substrate and quickly covered with another piece of cleaved mica slice. The layered assemblage was then placed on a hot plate and heated to 30 °C for more than 10 h to achieve quasi-static solution growth (Supporting Information S1). The ultrathin perovskite sheets grew on the mica, and those ultrathin perovskite sheets usually have a thickness from 10 to 100 nm and a lateral size larger than 10 μm. Actually by adjusting the volume of solvent, heating temperature, and growth time, the thickness and the area of the sheets could be tuned. For example, if 12 μL of precursor solution is applied, the grown perovskite sheets have the thickness from 100−400 nm, and the lateral size larger than 50 μm.

Characterizations. Optical micrographs and fluorescence images of the sheets were obtained with an optical microscope (ECLIPSE 80i, Nikon, Tokyo, Japan). Sheet morphology and thickness were measured with a Multimode atomic force microscope (AFM, Digital Instruments, Tonawanda, NY) in tapping mode. Crystallographic data were obtained with an ARL X'TRA powder diffractometer (Thermo Scientific, Waltham, MA). Field-emission scanning electron microscopy (FE-SEM) was performed with a Sigma 300 SEM (Zeiss, Oberkochen, Germany). Elemental distribution in the sheets was analyzed by energy dispersive X-ray spectroscopy with an EDS X-Max Extreme silicon drift detector (Oxford Instruments, Abingdon, U.K.) attached to the SEM system.

Optical Properties and Stability. Steady-state transmission spectra and absorption spectra were obtained with a 20/30 PV microspectrophotometer (CRAIC Technologies, San Dimas, CA). Spectra were collected with a 10× objective lens over a 15 μm^2 area using the mica substrate as a reference

https://dx.doi.org/10.1021/acs.nanolett.0c02468
Nano Lett. 2020, 20, 7144−7151

for background subtraction, while an objective lens with a numerical aperture of 0.2 was used to exclude the influence of the wide-angle reflection. Steady-state photoluminescence was measured using a confocal micro-Raman system (Princeton Instruments, Trenton, NJ). A WhiteLase SC400 supercontinuum fiber laser source (Fianium, Southampton, U.K.) was used for sample excitation at 488 nm. The samples were fixed on the outer jaws of a vernier caliper and flexed at various bending radii by decreasing the space between the jaws.

Device Fabrication and Measurement. The photodetector was fabricated by evaporating 80 nm thick Au electrodes onto 20 nm thick $MAPbBr_3$ nanosheets covered with patterned Si shadow masks. The active area of the photodetector ranges from 30 μm^2 to 100 μm^2 (Supporting Information S3). Here the active area of the photodetector is ~36 μm^2. The electrodes extended to the copper tape adhesive at the edge of the samples to reduce the influence of the measurements, and all of the measurements (except the measurements of moisture stability in Supporting Information S3) were performed in ambient condition at room temperature (24 °C) and ~40% humidity. The photocurrents were measured using a pair of tungsten steel probes connected to a 2636B SourceMeter (Keithley Instruments, Cleveland, OH). Illumination was provided by a 514 nm CW laser (Spectra-Physics, Santa Clara, CA) to measure the photoresponses under the flat state and bending states, respectively. A mode-locked Ti:sapphire laser (Spectra-Physics, MaiTai HP) with a BBO crystal was used to measure the response time and 3 dB bandwidth, and a broadband halogen lamp (10.5 mW/cm^2, Thorlabs, OSL-2) with collimator (Thorlabs, OSL2COL) was employed to measure the flexibility and bending stability of the sample with different thickness. Light modulation was carried out with a chopper (ThorLabs, Newton, NJ) with tunable frequency and an acoustic optical modulator (Gooch & Housego, I-M080).

The responsivity is determined by

$$R = \frac{\Delta I}{P \cdot S} = \frac{I_{light} - I_{dark}}{P \cdot S}$$

where I_{light} is the illuminated current and I_{dark} is the dark current, P is the laser power density, and S is the active area of PD.

■ ASSOCIATED CONTENT

Supporting Information

The Supporting Information is available free of charge at https://pubs.acs.org/doi/10.1021/acs.nanolett.0c02468.

Quasi-static synthesis process is discussed in detail; additional detailed characterization of the grown perovskite nanosheets, electric and optical measurement data, and photoelectrical response measurement data (PDF)

■ AUTHOR INFORMATION

Corresponding Authors

Ruwen Peng − *National Laboratory of Solid State Microstructures, School of Physics, and Collaborative Innovation Center of Advanced Microstructures, Nanjing University, Nanjing 210093, China;* orcid.org/0000-0003-0424-2771; Email: rwpeng@nju.edu.cn

Ren-Min Ma − *State Key Lab for Mesoscopic Physics and Frontiers Science Center for Nano-optoelectronics, School of Physics, Peking University, Beijing 100871, China;* orcid.org/0000-0003-4199-5772; Email: renminma@pku.edu.cn

Mu Wang − *National Laboratory of Solid State Microstructures, School of Physics, and Collaborative Innovation Center of Advanced Microstructures, Nanjing University, Nanjing 210093, China;* Email: muwang@nju.edu.cn

Authors

Hao Jing − *National Laboratory of Solid State Microstructures, School of Physics, and Collaborative Innovation Center of Advanced Microstructures, Nanjing University, Nanjing 210093, China*

Jie He − *National Laboratory of Solid State Microstructures, School of Physics, and Collaborative Innovation Center of Advanced Microstructures, Nanjing University, Nanjing 210093, China*

Yi Zhou − *National Laboratory of Solid State Microstructures, School of Physics, and Collaborative Innovation Center of Advanced Microstructures, Nanjing University, Nanjing 210093, China*

Zhenqian Yang − *State Key Lab for Mesoscopic Physics and Frontiers Science Center for Nano-optoelectronics, School of Physics, Peking University, Beijing 100871, China*

Cheng-Yao Li − *National Laboratory of Solid State Microstructures, School of Physics, and Collaborative Innovation Center of Advanced Microstructures, Nanjing University, Nanjing 210093, China*

Yu Liu − *National Laboratory of Solid State Microstructures, School of Physics, and Collaborative Innovation Center of Advanced Microstructures, Nanjing University, Nanjing 210093, China*

Xiaojiao Guo − *State Key Laboratory of ASIC and System, School of Microelectronics, Fudan University, Shanghai 200433, China*

Yingying Zhu − *National Laboratory of Solid State Microstructures, School of Physics, and Collaborative Innovation Center of Advanced Microstructures, Nanjing University, Nanjing 210093, China*

Di Wang − *Institute of Functional Crystals, Tianjin University of Technology, Tianjin 300384, China;* orcid.org/0000-0002-7850-1601

Jing Su − *School of Physics and Optoelectronic Engineering, Nanjing University of Information Science and Technology, Nanjing 210044, China;* orcid.org/0000-0002-1812-5026

Cheng Sun − *Department of Mechanical Engineering, Northwestern University, Evanston, Illinois 60208, United States;* orcid.org/0000-0002-2744-0896

Wenzhong Bao − *State Key Laboratory of ASIC and System, School of Microelectronics, Fudan University, Shanghai 200433, China*

Complete contact information is available at: https://pubs.acs.org/10.1021/acs.nanolett.0c02468

Author Contributions

R.P., H.J., R.-M.M, and M.W. conceived this work. H.J. fabricated the device with the assistance of J.H., C.-Y.L., and Y.L.; H.J. performed the electrical and optical experiments with the assistance of Y.Z., Z.Y., and Y. Zhu.; D.W. and J.S. provided the precursor solution. W.B. and X.G. provided the Si shadow masks. C.S. helped to do the characteristic of the device. R.P., R.-M.M, and M.W. directed the experiments. H.J., R.-M.M., R.P., C.S., and M.W. wrote the manuscript.

https://dx.doi.org/10.1021/acs.nanolett.0c02468
Nano Lett. 2020, 20, 7144−7151

Notes

The authors declare no competing financial interest.

■ ACKNOWLEDGMENTS

This work is supported by the National Key R&D Program of China (2017YFA0303702), and by the National Natural Science Foundation of China (Grants 11634005, 11974177, 61975078, 11674155). R.-M.M. is supported by the National Natural Science Foundation of China (Grants 91950115, 11774014, 61521004), Beijing Natural Science Foundation (Grant Z180011) and the National Key R&D Program of China (Grant 2018YFA0704401).

■ REFERENCES

(1) Nathan, A.; Ahnood, A.; Cole, M. T.; Lee, S.; Suzuki, Y.; Hiralal, P.; Bonaccorso, F.; Hasan, T.; Garcia-Gancedo, L.; Dyadyusha, A.; Haque, S.; Andrew, P.; Hofmann, S.; Moultrie, J.; Chu, D.; Flewitt, A. J.; Ferrari, A. C.; Kelly, M. J.; Robertson, J.; Amaratunga, G. A. J.; Milne, W. I. Flexible Electronics: The Next Ubiquitous Platform. *Proc. IEEE* **2012**, *100*, 1486−1517.

(2) Kim, R. H.; Kim, S.; Song, Y. M.; Jeong, H.; Kim, T. I.; Lee, J.; Li, X.; Choquette, K. D.; Rogers, J. A. Flexible Vertical Light Emitting Diodes. *Small* **2012**, *8*, 3123−3128.

(3) García de Arquer, F. P.; Armin, A.; Meredith, P.; Sargent, E. H. Solution-processed semiconductors for next-generation photodetectors. *Nat. Rev. Mater.* **2017**, *2*, 16100.

(4) Gao, L. Flexible Device Applications of 2D Semiconductors. *Small* **2017**, *13*, 1603994.

(5) Fan, W.; Zeng, J.; Gan, Q.; Ji, D.; Song, H.; Liu, W.; Shi, L.; Wu, L. Iridescence-controlled and flexibly tunable retroreflective structural color film for smart displays. *Sci. Adv.* **2019**, *5*, No. eaaw8755.

(6) Wang, C.-C.; Trivedi, S. B.; Jin, F.; Stepanov, S.; Chen, Z.; Khurgin, J.; Rodriguez, P.; Prasad, N. S. Human Life Signs Detection Using High-Sensitivity Pulsed Laser Vibrometer. *IEEE Sens. J.* **2007**, *7*, 1370−1376.

(7) Liu, N.; Tian, H.; Schwartz, G.; Tok, J. B.; Ren, T. L.; Bao, Z. Large-Area, Transparent, and Flexible Infrared Photodetector Fabricated Using P-N Junctions Formed by N-Doping Chemical Vapor Deposition Grown Graphene. *Nano Lett.* **2014**, *14*, 3702−3708.

(8) De Fazio, D.; Goykhman, I.; Yoon, D.; Bruna, M.; Eiden, A.; Milana, S.; Sassi, U.; Barbone, M.; Dumcenco, D.; Marinov, K.; Kis, A.; Ferrari, A. C. High Responsivity, Large-Area Graphene/MoS_2 Flexible Photodetectors. *ACS Nano* **2016**, *10*, 8252−8262.

(9) Cho, B.; Yoon, J.; Lim, S. K.; Kim, A. R.; Kim, D. H.; Park, S. G.; Kwon, J. D.; Lee, Y. J.; Lee, K. H.; Lee, B. H.; Ko, H. C.; Hahm, M. G. Chemical Sensing of 2D Graphene/MoS_2 Heterostructure device. *ACS Appl. Mater. Interfaces* **2015**, *7*, 16775−16780.

(10) Liu, X.-M.; Wang, M.; Wang, F.; Xu, T.; Li, Y.-L.; Peng, X.-S.; Wei, H.-Y.; Guan, Z.-Y.; Zang, Z.-G. High-Performance Photodetectors with X-Ray Responsivity Based on Interface Modified Perovskite Film. *IEEE Electron Device Lett.* **2020**, *99*, 1.

(11) Wang, H.-X.; Zhang, P.-F.; Zang, Z.-G. High performance $CsPbBr_3$ quantum dots photodetectors by using zinc oxide nanorods arrays as an electron-transport layer. *Appl. Phys. Lett.* **2020**, *116*, 162103.

(12) Lee, M. M.; Teuscher, J.; Miyasaka, T.; Murakami, T. N.; Snaith, H. J. Efficient hybrid solar cells based on meso-superstructured organometal halide perovskites. *Science* **2012**, *338*, 643−647.

(13) Xing, G.; Mathews, N.; Sun, S.; Lim, S. S.; Lam, Y. M.; Grätzel, M.; Mhaisalkar, S.; Sum, T. C. Long-range balanced electron-and hole-transport lengths in organic-inorganic $CH_3NH_3PbI_3$. *Science* **2013**, *342*, 344−347.

(14) Eperon, G. E.; Stranks, S. D.; Menelaou, C.; Johnston, M. B.; Herz, L. M.; Snaith, H. J. Formamidinium lead trihalide: a broadly tunable perovskite for efficient planar heterojunction solar cells. *Energy Environ. Sci.* **2014**, *7*, 982−988.

(15) Stoumpos, C. C.; Malliakas, C. D.; Kanatzidis, M. G. Semiconducting tin and lead iodide perovskites with organic cations: phase transitions, high mobilities, and near-infrared photoluminescent properties. *Inorg. Chem.* **2013**, *52*, 9019−9038.

(16) Lin, K.; Xing, J.; Quan, L. N.; de Arquer, F. P. G.; Gong, X.; Lu, J.; Xie, L.; Zhao, W.; Zhang, D.; Yan, C.; Li, W.; Liu, X.; Lu, Y.; Kirman, J.; Sargent, E. H.; Xiong, Q.; Wei, Z. Perovskite light-emitting diodes with external quantum efficiency exceeding 20%. *Nature* **2018**, *562*, 245−248.

(17) Cao, Y.; Wang, N.; Tian, H.; Guo, J.; Wei, Y.; Chen, H.; Miao, Y.; Zou, W.; Pan, K.; He, Y.; Cao, H.; Ke, Y.; Xu, M.; Wang, Y.; Yang, M.; Du, K.; Fu, Z.; Kong, D.; Dai, D.; Jin, Y.; Li, G.; Li, H.; Peng, Q.; Wang, J.; Huang, W. Perovskite light-emitting diodes based on spontaneously formed submicrometre-scale structures. *Nature* **2018**, *562*, 249−253.

(18) Liu, D.; Kelly, T. L. Perovskite solar cells with a planar heterojunction structure prepared using room-temperature solution processing techniques. *Nat. Photonics* **2014**, *8*, 133−138.

(19) Li, G.; Tan, Z. K.; Di, D.; Lai, M. L.; Jiang, L.; Lim, J. H.; Friend, R. H.; Greenham, N. C. Efficient Light-Emitting Diodes Based on Nanocrystalline Perovskite in a Dielectric Polymer Matrix. *Nano Lett.* **2015**, *15*, 2640−2644.

(20) Docampo, P.; Ball, J. M.; Darwich, M.; Eperon, G. E.; Snaith, H. J. Efficient organometal trihalide perovskite planar-heterojunction solar cells on flexible polymer substrates. *Nat. Commun.* **2013**, *4*, 2761.

(21) Zhang, N.; Sun, W.; Rodrigues, S. P.; Wang, K.; Gu, Z.; Wang, S.; Cai, W.; Xiao, S.; Song, Q. Highly Reproducible Organometallic Halide Perovskite Microdevices based on Top-Down Lithography. *Adv. Mater.* **2017**, *29*, 1606205.

(22) Du, B.; Yang, W.; Jiang, Q.; Shan, H.; Luo, D.; Li, B.; Tang, W.; Lin, F.; Shen, B.; Gong, Q.; Zhu, X.; Zhu, R.; Fang, Z. Plasmonic-Functionalized Broadband Perovskite Photodetector. *Adv. Opt. Mater.* **2018**, *6*, 1701271.

(23) Hu, X.; Zhang, X.; Liang, L.; Bao, J.; Li, S.; Yang, W.; Xie, Y. High-Performance Flexible Broadband Photodetector Based on Organolead Halide Perovskite. *Adv. Funct. Mater.* **2014**, *24*, 7373−7380.

(24) Bao, C.; Zhu, W.; Yang, J.; Li, F.; Gu, S.; Wang, Y.; Yu, T.; Zhu, J.; Zhou, Y.; Zou, Z. Highly Flexible Self-Powered Organolead Trihalide Perovskite Photodetectors with Gold Nanowire Networks as Transparent Electrodes. *ACS Appl. Mater. Interfaces* **2016**, *8*, 23868−23875.

(25) Deng, W.; Zhang, X.; Huang, L.; Xu, X.; Wang, L.; Wang, J.; Shang, Q.; Lee, S. T.; Jie, J. Aligned Single-Crystalline Perovskite Microwire Arrays for High-Performance Flexible Image Sensors with Long-Term Stability. *Adv. Mater.* **2016**, *28*, 2201−2208.

(26) Gu, L.; Tavakoli, M. M.; Zhang, D.; Zhang, Q.; Waleed, A.; Xiao, Y.; Tsui, K. H.; Lin, Y.; Liao, L.; Wang, J.; Fan, Z. 3D Arrays of 1024-Pixel Image Sensors based on Lead Halide Perovskite Nanowires. *Adv. Mater.* **2016**, *28*, 9713−9721.

(27) Sun, H.; Lei, T.; Tian, W.; Cao, F.; Xiong, J.; Li, L. Self-Powered, Flexible, and Solution-Processable Perovskite Photodetector Based on Low-Cost Carbon Cloth. *Small* **2017**, *13*, 1701042.

(28) Sun, H.; Tian, W.; Cao, F.; Xiong, J.; Li, L. Ultrahigh-Performance Self-Powered Flexible Double-Twisted Fibrous Broadband Perovskite Photodetector. *Adv. Mater.* **2018**, *30*, 1706986.

(29) Fang, Y.; Dong, Q.; Shao, Y.; Yuan, Y.; Huang, J. Highly narrowband perovskite single-crystal photodetectors enabled by surface-charge recombination. *Nat. Photonics* **2015**, *9*, 679−686.

(30) Shi, D.; Adinolfi, V.; Comin, R.; Yuan, M.; Alarousu, E.; Buin, A.; Chen, Y.; Hoogland, S.; Rothenberger, A.; Katsiev, K.; Losovyj, Y.; Zhang, X.; Dowben, P. A.; Mohammed, O. F.; Sargent, E. H.; Bakr, O. M. Low trap-state density and long carrier diffusion in organolead trihalide perovskite single crystals. *Science* **2015**, *347*, 519−522.

(31) Fu, Y.; Meng, F.; Rowley, M. B.; Thompson, B. J.; Shearer, M. J.; Ma, D.; Hamers, R. J.; Wright, J. C.; Jin, S. Solution Growth of Single Crystal Methylammonium Lead Halide Perovskite Nanostruc-

https://dx.doi.org/10.1021/acs.nanolett.0c02468
Nano Lett. 2020, 20, 7144−7151

tures for Optoelectronic and Photovoltaic Applications. *J. Am. Chem. Soc.* **2015**, *137*, 5810−5818.
(32) Yuan, Y.; Huang, J. Ion Migration in Organometal Trihalide Perovskite and Its Impact on Photovoltaic Efficiency and Stability. *Acc. Chem. Res.* **2016**, *49*, 286−293.
(33) Li, X.; Dar, M. I.; Yi, C.; Luo, J.; Tschumi, M.; Zakeeruddin, S. M.; Nazeeruddin, M. K.; Han, H.; Gratzel, M. Improved performance and stability of perovskite solar cells by crystal crosslinking with alkylphosphonic acid ω-ammonium chlorides. *Nat. Chem.* **2015**, *7*, 703−711.
(34) Yang, Z.; Deng, Y.; Zhang, X.; Wang, S.; Chen, H.; Yang, S.; Khurgin, J. B.; Fang, N. X.; Zhang, X.; Ma, R. High-Performance Single-Crystalline Perovskite Thin-Film Photodetector. *Adv. Mater.* **2018**, *30*, 1704333.
(35) Gu, Z.; Huang, Z.; Li, C.; Li, M.; Song, Y. A general printing approach for scalable growth of perovskite single-crystal films. *Sci. Adv.* **2018**, *4*, No. eaat2390.
(36) Yang, T.; Zhao, Y. L.; Tong, Y.; Jiao, Z. B.; Wei, J.; Cai, J. X.; Han, X. D.; Chen, D.; Hu, A.; Kai, J. J.; Lu, K.; Liu, Y.; Liu, C. T. Multicomponent intermetallic nanoparticles and superb mechanical behaviors of complex alloys. *Science* **2018**, *362*, 933−937.
(37) Wang, Q.; Wang, J.; Li, J.; Zhang, Z.; Mao, S. X. Consecutive crystallographic reorientations and superplasticity in body-centered cubic niobium nanowires. *Sci. Adv.* **2018**, *4*, No. eaas8850.
(38) Banerjee, A.; Bernoulli, D.; Zhang, H.; Yuen, M.-F.; Liu, J.; Dong, J.; Ding, F.; Lu, J.; Dao, M.; Zhang, W.; Lu, Y.; Suresh, S. Ultralarge elastic deformation of nanoscale diamond. *Science* **2018**, *360*, 300−302.
(39) Song, J.; Xu, L.; Li, J.; Xue, J.; Dong, Y.; Li, X.; Zeng, H. Monolayer and Few-Layer All-Inorganic Perovskites as a New Family of Two-Dimensional Semiconductors for Printable Optoelectronic Devices. *Adv. Mater.* **2016**, *28*, 4861−4869.
(40) Leung, S. F.; Ho, K. T.; Kung, P. K.; Hsiao, V. K. S.; Alshareef, H. N.; Wang, Z. L.; He, J. H. A Self-Powered and Flexible Organometallic Halide Perovskite Photodetector with Very High Detectivity. *Adv. Mater.* **2018**, *30*, 1704611.
(41) Hu, W.; Huang, W.; Yang, S.; Wang, X.; Jiang, Z.; Zhu, X.; Zhou, H.; Liu, H.; Zhang, Q.; Zhuang, X.; Yang, J.; Kim, D. H.; Pan, A. High-Performance Flexible Photodetectors based on High-Quality Perovskite Thin Films by a Vapor−Solution Method. *Adv. Mater.* **2017**, *29*, 1703256.
(42) Li, J.; Shen, Y.; Liu, Y.; Shi, F.; Ren, X.; Niu, T.; Zhao, K.; Liu, S. F. Stable High-Performance Flexible Photodetector Based on Upconversion Nanoparticles/Perovskite Microarrays Composite. *ACS Appl. Mater. Interfaces* **2017**, *9*, 19176−19183.
(43) Wang, M.; Zhong, S.; Yin, X.-B.; Zhu, J.-M.; Peng, R.-W.; Wang, Y.; Zhang, K.-Q.; Ming, N.-B. Nanostructured copper filaments in electrochemical deposition. *Phys. Rev. Lett.* **2001**, *86*, 3827−3830.
(44) Chen, Y.-X.; Ge, Q.-Q.; Shi, Y.; Liu, J.; Xue, D.-J.; Ma, J.-Y.; Ding, J.; Yan, H.-J.; Hu, J.-S.; Wan, L.-J. General space-confined on-substrate fabrication of thickness-adjustable hybrid perovskite single-crystalline thin films. *J. Am. Chem. Soc.* **2016**, *138*, 16196−16199.
(45) Chen, Z.-L.; Dong, Q.-F.; Liu, Y.; Bao, C.-X.; Fang, Y.-J.; Lin, Y.; Tang, S.; Wang, Q.; Xiao, X.; Bai, Y.; Deng, Y.-H.; Huang, J.-S. Thin single crystal perovskite solar cells to harvest below-bandgap light absorption. *Nat. Commun.* **2017**, *8*, 1890.
(46) Zhang, B.; Weng, Y.-Y.; Huang, X.-P.; Wang, M.; Peng, R.-W.; Ming, N.-B.; Yang, B.; Lu, N.; Chi, L. Creating In-Plane Metallic-Nanowire Arrays by Corner-Mediated Electrodeposition. *Adv. Mater.* **2009**, *21*, 3576−3580.
(47) Ke, S.; Chen, C.; Fu, N.; Zhou, H.; Ye, M.; Lin, P.; Yuan, W.; Zeng, X.; Chen, L.; Huang, H. Transparent Indium Tin Oxide Electrodes on Muscovite Mica for High-Temperature-Processed Flexible Optoelectronic Devices. *ACS Appl. Mater. Interfaces* **2016**, *8*, 28406−28411.
(48) Schultz, J.; Tsutsumi, K.; Donnet, J.-B. Surface properties of high-energy solids: II. Determination of the nondispersive component of the surface free energy of mica and its energy of adhesion to polar liquids. *J. Colloid Interface Sci.* **1977**, *59*, 277−282.
(49) Wang, Y.; Shi, Y.; Xin, G.; Lian, J.; Shi, J. Two-Dimensional van der Waals Epitaxy Kinetics in a Three Dimensional Perovskite Halide. *Cryst. Growth Des.* **2015**, *15*, 4741−4749.
(50) Peng, W.; Wang, L.; Murali, B.; Ho, K. T.; Bera, A.; Cho, N.; Kang, C. F.; Burlakov, V. M.; Pan, J.; Sinatra, L.; Ma, C.; Xu, W.; Shi, D.; Alarousu, E.; Goriely, A.; He, J. H.; Mohammed, O. F.; Wu, T.; Bakr, O. M. Solution-Grown Monocrystalline Hybrid Perovskite Films for Hole-Transporter-Free Solar Cells. *Adv. Mater.* **2016**, *28*, 3383−3390.
(51) Dou, L.; Yang, Y. M.; You, J.; Hong, Z.; Chang, W. H.; Li, G.; Yang, Y. Solution-processed hybrid perovskite photodetectors with high detectivity. *Nat. Commun.* **2014**, *5*, 5404.
(52) Xie, C.; Yan, F. Flexible Photodetectors Based on Novel Functional Materials. *Small* **2017**, *13*, 1701822.
(53) Fang, Y.-J.; Armin, A.; Meredith, P.; Huang, J.-S. Accurate characterization of next-generation thin-film photodetectors. *Nat. Photonics* **2019**, *13*, 1−4.
(54) Deng, H.; Yang, X.; Dong, D.; Li, B.; Yang, D.; Yuan, S.; Qiao, K.; Cheng, Y. B.; Tang, J.; Song, H. Flexible and Semitransparent Organolead Triiodide Perovskite Network Photodetector Arrays with High Stability. *Nano Lett.* **2015**, *15*, 7963−7969.
(55) Li, X.; Yu, D.; Chen, J.; Wang, Y.; Cao, F.; Wei, Y.; Wu, Y.; Wang, L.; Zhu, Y.; Sun, Z.; Ji, J.; Shen, Y.; Sun, H.; Zeng, H. Constructing Fast Carrier Tracks into Flexible Perovskite Photodetectors to Greatly Improve Responsivity. *ACS Nano* **2017**, *11*, 2015−2023.
(56) Adams, G. R.; Adhikari, N.; Parker, H.; Okoli, O. Flexible Wire-Shaped Perovskite Photodetector via Joule Heating for Improved Crystallization and Performance. *Adv. Mater. Interfaces* **2018**, *5*, 1800082.
(57) Zheng, W.; Xiong, X.; Lin, R.; Zhang, Z.; Xu, C.; Huang, F. Balanced Photodetection in One-Step Liquid-Phase-Synthesized $CsPbBr_3$ Micro-/Nanoflake Single Crystals. *ACS Appl. Mater. Interfaces* **2018**, *10*, 1865−1870.
(58) Liu, Y.; Zhang, Y.; Yang, Z.; Ye, H.; Feng, J.; Xu, Z.; Zhang, X.; Munir, R.; Liu, J.; Zuo, P.; Li, Q.; Hu, M.; Meng, L.; Wang, K.; Smilgies, D. M.; Zhao, G.; Xu, H.; Yang, Z.; Amassian, A.; Li, J.; Zhao, K.; Liu, S. F. Multi-inch single-crystalline perovskite membrane for high-detectivity flexible photosensors. *Nat. Commun.* **2018**, *9*, 5302.
(59) Cen, G.; Liu, Y.; Zhao, C.; Wang, G.; Fu, Y.; Yan, G.; Yuan, Y.; Su, C.; Zhao, Z.; Mai, W. Atomic-Layer Deposition-Assisted Double-Side Interfacial Engineering for High-Performance Flexible and Stable $CsPbBr_3$ Perovskite Photodetectors toward Visible Light Communication Applications. *Small* **2019**, *15*, 1902135.
(60) Asuo, I. M.; Fourmont, P.; Ka, I.; Gedamu, D.; Bouzidi, S.; Pignolet, A.; Nechache, R.; Cloutier, S. G. Highly Efficient and Ultrasensitive Large-Area Flexible Photodetector Based on Perovskite Nanowires. *Small* **2019**, *15*, 1804150.
(61) Deng, W.; Huang, H.; Jin, H.; Li, W.; Chu, X.; Xiong, D.; Yan, W.; Chun, F.; Xie, M.; Luo, C.; Jin, L.; Liu, C.; Zhang, H.; Deng, W.; Yang, W. All-Sprayed-Processable, Large-Area, and Flexible Perovskite /MXene-Based Photodetector Arrays for Photocommunication. *Adv. Opt. Mater.* **2019**, *7*, 1801521.
(62) Xia, H.; Tong, S.; Zhang, C.; Wang, C.; Sun, J.; He, J.; Zhang, J.; Gao, Y.; Yang, J. Flexible and air-stable perovskite network photodetectors based on $CH_3NH_3PbI_3$/C8BTBT bulk heterojunction. *Appl. Phys. Lett.* **2018**, *112*, 233301.
(63) Liu, Z.; You, P.; Xie, C.; Tang, G.; Yan, F. Ultrathin and flexible perovskite solar cells with graphene transparent electrode. *Nano Energy* **2016**, *28*, 151−157.
(64) Rolston, N.; Printz, A. D.; Tracy, J. M.; Weerasinghe, H. C.; Vak, D.; Haur, L. J.; Priyadarshi, A.; Mathews, N.; Slotcavage, D. J.; McGehee, M. D.; Kalan, R. E.; Zielinski, K.; Grimm, R. L.; Tsai, H.; Nie, W.; Mohite, A. D.; Gholipour, S.; Saliba, M.; Grätzel, M.; Dauskardt, R. H. Effect of Cation Composition on the Mechanical Stability of Perovskite Solar Cells. *Adv. Energy Mater.* **2018**, *8*, 1702116.
(65) Akinwande, D.; Petrone, N.; Hone, J. Two-dimensional flexible nanoelectronics. *Nat. Commun.* **2014**, *5*, 5678.

https://dx.doi.org/10.1021/acs.nanolett.0c02468
Nano Lett. 2020, 20, 7144−7151